AGU ADVANCING EARTH AND SPACE SCIENCE

Geophysical Research Letters

RESEARCH LETTER
10.1029/2020GL090865

Key Points:

- Rare multiyear tall tower and ground-based ammonia measurements were combined with WRF-Chem to constrain emissions from the US Corn Belt
- Monthly ammonia emissions peaked in May through July and were 1.6–1.7 times the annual NEI average
- Episodic low WRF-Chem bias versus tall tower observations underscore the importance of weather and land management as emission drivers

Supporting Information:

- Supporting Information S1

Correspondence to:
C. Hu and T. J. Griffis,
huxxx991@umn.edu or
nihaohucheng@163.com;
timgriffis@umn.edu

Citation:
Hu, C., Griffis, T. J., Frie, A., Baker, J. M., Wood, J. D., Millet, D. B., et al. (2021). A multiyear constraint on ammonia emissions and deposition within the US Corn Belt. *Geophysical Research Letters*, *48*, e2020GL090865. https://doi.org/10.1029/2020GL090865

Received 18 SEP 2020
Accepted 27 JAN 2021

A Multiyear Constraint on Ammonia Emissions and Deposition Within the US Corn Belt

Cheng Hu[1,2], Timothy J. Griffis[2], Alexander Frie[2], John M. Baker[2,3], Jeffrey D. Wood[4], Dylan B. Millet[2], Zhongjie Yu[2], Xueying Yu[2], and Alan C. Czarnetzki[5]

[1]College of Biology and the Environment, Joint Center for Sustainable Forestry in Southern China, Nanjing Forestry University, Nanjing, China, [2]Department of Soil, Water, and Climate, University of Minnesota-Twin Cities, St. Paul, MN, USA, [3]United States Department of Agriculture – Agriculture Research Service, St. Paul, MN, USA, [4]School of Natural Resources, University of Missouri, Columbia, MO, USA, [5]Department of Earth and Environmental Sciences, University of Northern Iowa, Cedar Falls, IA, USA

Abstract The US Corn Belt is a global hotspot of atmospheric ammonia (NH_3), a gas known to adversely impact the environment and human health. We combine hourly tall tower (100 m) measurements and bi-weekly, spatially distributed, ground-based observations from the Ammonia Monitoring Network with the US National Emissions Inventory (NEI) and WRF-Chem simulations to constrain NH_3 emissions from April to September 2017–2019. We show that: (1) NH_3 emissions peaked from May to July and were 1.6–1.7 times the annual NEI average; (2) average growing season NH_3 emissions from agricultural lands were remarkably similar across years (3.27–3.64 nmol m^{-2} s^{-1}), yet showed substantial episodic variability driven by meteorology and land management; (3) dry deposition was 40% of gross emissions from agricultural lands and exceeded 100% of gross emissions in natural lands. Our findings provide an important benchmark for evaluating future NH_3 emissions and mitigation efforts.

1. Introduction

As global demand for food, fiber, and biofuels rises, the upstream application of nitrogen fertilizer and production of livestock have also increased. Coinciding with these increases, ammonia (NH_3) emissions have risen by 500% in the past century and are projected to increase by 50% between 2000 and 2050 (Bouwman et al., 2013; Warner et al., 2017; Yu et al., 2018). Atmospheric NH_3 has been associated with negative human health and environmental impacts, including eutrophication/acidification and biodiversity loss (Galloway et al., 2008; Sebestyen et al., 2019; Sutton et al., 2013). Dry deposition of NH_3 emitted from agricultural sources often drives these adverse impacts on natural ecosystems (Sheppard et al., 2011; Warner et al., 2017). There is a need, therefore, for robust evaluation of NH_3 emissions and dry deposition within agricultural regions.

In the United States (US), the Corn Belt is considered an NH_3 emission hotspot (Li et al., 2016; Paulot et al., 2014; Warner et al., 2017), accounting for ~35% of US agricultural NH_3 emissions in 2014 (EPA, 2014). Relatively few regional-scale studies have attempted to quantify US Corn Belt NH_3 emissions. Previous efforts to constrain emissions in this region have utilized a number of different approaches (Gilliland et al., 2003; Griffis et al., 2019; Paulot et al., 2014; Zhu et al., 2013); despite these efforts, regional NH_3 emission uncertainty still remains high (i.e., from 20% to >50%, see supporting information) in terms of both the seasonality and magnitude. Further, few studies have attempted to quantify multiyear emissions and deposition fluxes for this region (Li et al., 2016).

Many factors drive NH_3 emission uncertainties. Flux observations show that NH_3 emissions respond strongly to environmental conditions including soil properties, air temperature, and canopy characteristics (Bash et al., 2013; Shonkwiler & Ham, 2018; Walker et al., 2012). However, many inventories, including the US National Emissions Inventory (NEI, https://www.epa.gov/air-emissions-inventories/), do not incorporate the dynamics of local environmental conditions into emission estimates (Goebes et al., 2003). Errors can also arise from uncertainties in the spatial distribution of emissions, local fertilizer/manure application times, and emission factors (EFs). For example, one analysis estimated the EF of nitrogen solutions at 3.2%, much smaller than the 8% used in the NEI (Balasubramanian et al., 2015, 2017). An additional understudied source of uncertainty is the seasonal and interannual variability of NH_3 emissions, deposition, and

atmospheric concentrations. Given the above issues, there is a continuing need to evaluate NH_3 emission estimates with multiyear observations to help benchmark regional emissions.

One approach to reducing the uncertainty in NH_3 inventories is through high temporal resolution NH_3 observations. Most of the atmospheric physical/chemical processes affecting NH_3, such as emission, aerosol uptake, and deposition occur on hourly timescales (Ackerman et al., 2019; Dammers et al., 2019). Field measurements of NH_3 can thus be used to constrain emissions on a local-to-regional scale (Bie et al., 2018; Fu et al., 2017). High frequency NH_3 observations from tall towers have the potential to improve regional NH_3 emission estimates due to their greater spatial footprint and higher temporal resolution than traditional ground-based filter observations (Hu et al., 2019; Moravek et al., 2019). The large spatial footprint also helps minimize aggregation error when comparing tall tower observations with modeled concentrations. However, tall tower atmospheric NH_3 observations remain relatively rare in the US (Griffis et al., 2019; Tevlin et al., 2017) and elsewhere (Dammers et al., 2017).

The Corn Belt is estimated to have the highest nitrogen deposition rates in the US, with dry NH_3 deposition accounting for approximately 50% of the total N deposition (Li et al., 2016). The interannual NH_3 variability over this hotspot and the resulting impacts on atmospheric NH_3 distributions and downwind deposition remain poorly quantified (Heald et al., 2012; Li et al., 2016; Schiferl et al., 2016; Walker et al., 2012). Our previous work evaluated regional NH_3 emissions in November of 2017 and 2018, and demonstrated that multiyear tall tower NH_3 observations can provide valuable insights into NH_3 emissions and dry deposition (Hu et al., 2019). Here, we combine three years of tall-tower data and ground-level NH_3 observations with chemical transport model (WRF-Chem) simulations to: (1) constrain NH_3 emissions in the US Corn Belt during the growing season (April to September) and their interannual variability; and (2) Investigate the magnitude of NH_3 dry deposition downwind of agricultural regions. Such efforts are needed to constrain NH_3 budgets and to provide an evaluation benchmark for future NH_3 mitigation efforts.

2. Materials and Methods

2.1. Tall Tower Site

The US Corn Belt is defined here as all or parts of Minnesota, Iowa, Illinois, Missouri, Ohio, Indiana, South Dakota, Wisconsin, and Nebraska. In this region, the primary agricultural practice is corn-soybean rotation (Green et al., 2017). Atmospheric NH_3 concentrations were measured at 100 and 56 m above ground level at the KCMP tall tower (44.689°N, 93.073°W, tower base is 290 m above sea level), which is located near the northern border of the US Corn Belt in Minnesota (Griffis et al., 2019; Figure 1a). According to the US Department of Agriculture Cropland Data Layer data for 2019, land use within the tall tower main concentration footprint (i.e., ~100 km radius) consists of 42% cropland, 38% natural land (forests, pasture, and grassland), and 20% developed lands or open water.

2.2. WRF-CHEM Modeling

We used the Weather Research and Forecasting with Chemistry (WRF-Chem, version 3.9.1.1) model to simulate NH_3 mixing ratios and other atmospheric chemical and physical parameters from April 1 to September 30 in years 2017–2019. Three nested spatial domains were used, with horizontal resolutions of 45, 15, and 5 km following Hu et al. (2019). WRF-Chem employs the Carbon Bond Mechanism version Z (CBMZ without DMS) and the MOSAIC gas-particle partitioning module (Zaveri et al., 2008). Annual anthropogenic emissions for years 2017–2019 were derived by scaling the NEI 2011 inventory according to EPA annual emission trends between 2011 and 2017. Since the scaling data was unavailable for 2018 and 2019 when this study was conducted, the scaled 2017 emissions were used for all years. Monthly NH_3 emission variations (which are not included in NEI) were incorporated based on the EDGAR (Emission Database for Global Atmospheric Research, Olivier et al., 1994) htap v2 data set (Table S1) for the year of 2012, with the normalized EDGAR seasonality applied to the annual NEI data to derive the monthly *a priori* emissions, which are the same for each year. We have selected htap v2 because it provided more reasonable monthly variations than the other EDGAR products and is also consistent with our previous work (Hu et al., 2019). The uncertainties in the *a priori* NH_3 emissions and the influence of not accounting for bi-directional flux in WRF-Chem are also discussed in the supporting information.

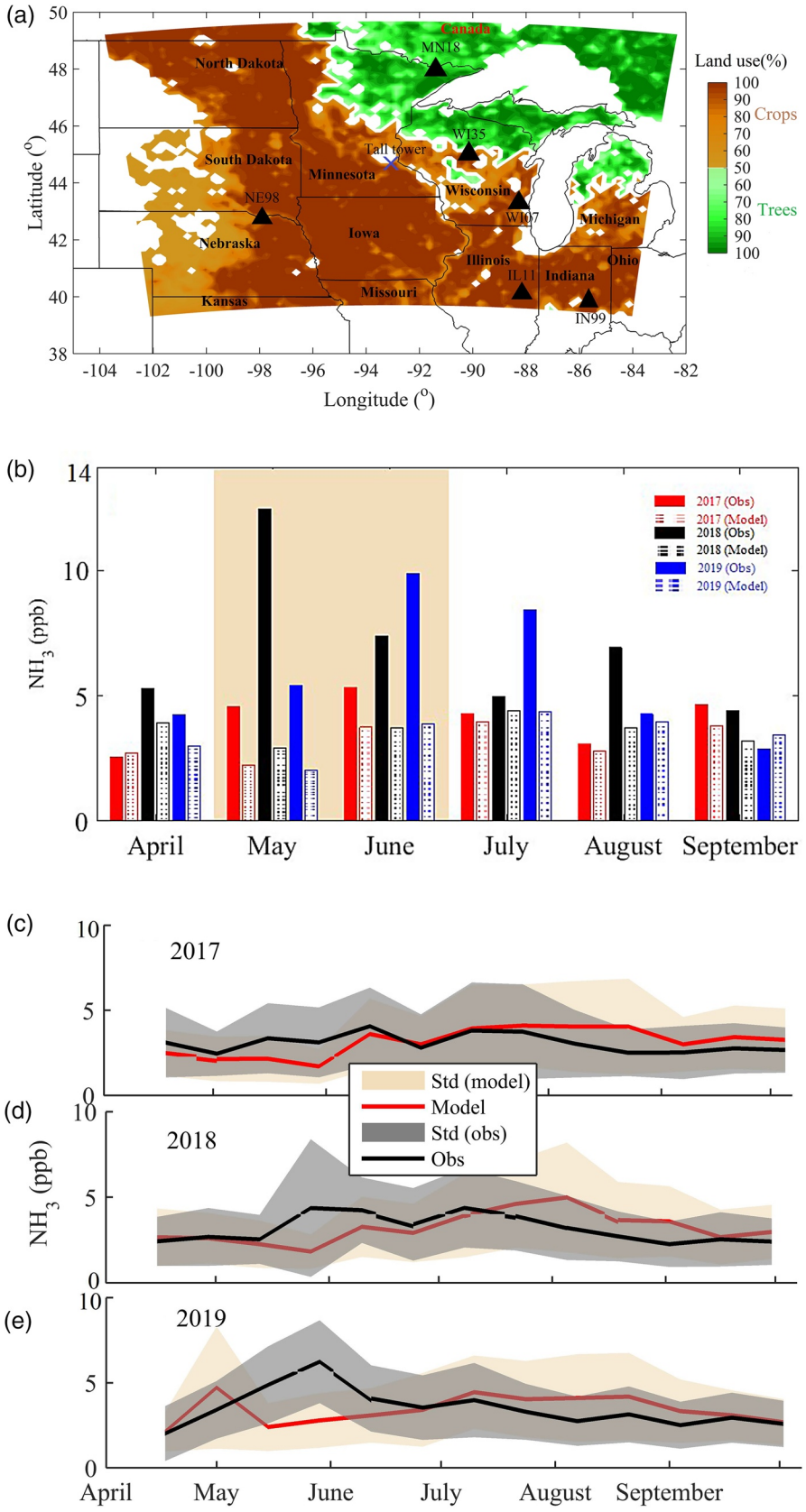
(a)
Canada
MN18
North Dakota
WI35
Tall tower
South Dakota
Minnesota
Wisconsin
NE98
WI07
Michigan
Nebraska
Iowa
Illinois
Ohio
IL11
Indiana
Missouri
Kansas
IN99
Land use(%)
Crops
Trees
Latitude (°)
Longitude (°)
(b)
2017 (Obs)
2017 (Model)
2018 (Obs)
2018 (Model)
2019 (Obs)
2019 (Model)
NH3 (ppb)
April
May
June
July
August
September
(c)
2017
(d)
2018
(e)
2019
Std (model)
Model
Std (obs)
Obs

2.3. NH_3 Mixing Ratio Observations

Tall tower NH_3 mixing ratios have been measured near-continuously at 100 m since March 2017 and continue as of December 11, 2020 (for details see Griffis et al., 2019). Air samples are pulled continuously down the tower, subsampled, and measured using an off-axis cavity ring-down spectrometer (EAA-30-EP, Los Gatos Research, San Jose, CA, USA). The measurement apparatus has a precision of 0.25 ppb over a 100 s averaging period (Griffis et al., 2019). Hourly and daily average mixing ratio values were used for comparisons with model results. In addition, bi-weekly ground-level NH_3 observations from six Atmospheric Ammonia Network (AMoN) sites were used to evaluate NH_3 spatial distributions simulated by WRF-Chem, which represents the average NH_3 every 2 weeks. Seven AMoN sites are located within Domain 2 (Figure 1a), but because 2 months of observations were unavailable for the IL37 site, it was not used in this study. Three of the sites are located within Domain 3. The six sites represent distinct land uses including: remote forest/grassland (MN18, WI07), urban (IN99), and agricultural (WI35, NE98, IL11) (Yu et al., 2018). Although Yu et al. (2018) classified WI07 (a wetland site) as remote, ~37% of its surrounding area (i.e., within 50 km) is occupied by agricultural fields (Figure S1). We therefore classify it as an agricultural site (Section 3.2).

2.4. Model Evaluation

Previous work has shown that the WRF-Chem configuration above can reasonably represent several key diagnostic variables for our region of study including $PM_{2.5}$, 2 m air temperature (T_{2m}), relative humidity (RH), wind speed (WS), and wind direction (WD) (Hu et al., 2019). Further details and statistics regarding these variables and planetary boundary layer height (PBLH) observations and simulations are shown in the supporting information (Figures S2–S4, Table S2).

3. Results and Discussion

3.1. Observed and Modeled Hourly NH_3 Mixing Ratios

Observed hourly NH_3 mixing ratios at 100 m are compared with WRF-Chem predictions in Figure S5. The model generally captured the observed variability in NH_3 concentrations (with some notable exceptions during May to June in 2018 and May to July in 2019), with the root mean square error (RMSE) of 3.68, 6.86, and 5.10 ppb and coefficient of determination (R^2) of 0.30, 0.10, and 0.28 for 2017, 2018, and 2019, respectively. These analyses demonstrate the ability of WRF-Chem to capture the influence of weather patterns and atmospheric physical/chemical processes. We observed some episodic spikes in NH_3 mixing ratios that were not captured by the model, possibly caused by the inability of the prescribed monthly emissions to represent the true dynamics of changes in hourly emissions for some special conditions. Larger model-measurement discrepancies are seen during the months of May and June. When excluding these months, the RMSE decreased to 2.24, 5.36, and 4.21 ppb and the R^2 increased to 0.34, 0.17, and 0.30 for 2017, 2018, and 2019, respectively. For the daily averages, the R^2 increased to 0.53, 0.25, and 0.44, respectively, and the RMSE decreased to 2.12, 4.46, and 3.71, indicating better performance at longer time scales. Overall, these results point to a low model bias in the *a priori* emissions for these months as discussed later in Section 3.2.

Since the tall tower is located within a transition zone between an agricultural and nonagricultural region (Figure 1a), changes in wind direction can be used to diagnose NH_3 source contributions. To this end, NH_3 wind direction roses were calculated using both observed and simulated NH_3 mixing ratios (Figure S6a–S6f). The simulations show lower NH_3 mixing ratios for northerly winds, suggesting the relatively low NH_3 emissions from the forested and developed areas north of the site. Higher NH_3 mixing ratios were simulated during southerly winds, showing the influence of higher NH_3 emissions from the agricultural regions south of the site. In the tall tower NH_3 observations, similar wind direction trends were observed in 2017

Figure 1. (a) Land use categories for agricultural and forest area proportion within the study domain with the tall tower location displayed with a blue "x." AMoN sites are shown as black triangles; (b) model-measurement comparisons of monthly mean NH_3 mixing ratios (shading is added to highlight large model—measurement discrepancy in May and June); and time series averages across the six sites with shaded standard deviations for (c) 2017, (d) 2018, and (e) 2019.

(Figure S6a). Directional trends were less clear in the observations from 2018 to 2019 when much larger NH_3 values occurred in the observations than simulations, indicating potential bias of the *a priori* NH_3 emissions, that is, the on-road vehicle NH_3 emissions in north Saint-Paul-Minneapolis Metropolitan area. Statistical distributions of both observed and simulated NH_3 mixing ratios (Figure S6g) show that most hourly values fell between 1 and 3 ppb, with observations during 2018 and 2019 exhibiting a much higher frequency of elevated NH_3 concentrations than predicted by WRF-Chem.

3.2. Bi-weekly and Monthly NH_3 Mixing Ratios

Comparisons between observed and simulated monthly mean NH_3 mixing ratios are shown in Figure 1b and Table S3. The model results exhibit relatively little interannual variability, with the largest relative difference (44%) between April 2017 and 2018. Within the observations, greater monthly interannual variations were observed. Since the same *a priori* emissions are used in the model for a given month regardless of year, simulated interannual differences are driven mainly by atmospheric physical/chemical processes and weather patterns. As a result, the strong model underestimate of interannual NH_3 variability points to emission fluctuations as the primary driver of the observed interannual variability, assuming the model simulated physical/chemical processes have relatively small bias, which will be discussed in greater detail below.

AMoN observations were compared with WRF-Chem predictions by averaging the model output over the bi-weekly sampling intervals (Figures S7a–S7c). For each year, ~78 observations (13 observations for each site) were used. These comparisons illustrate the general agreement of the WRF-Chem output with AMoN data, which is slightly better than for the higher resolution tall tower data. This is because the high-frequency variability in emissions and atmospheric physical/chemical dynamics is smoothed by averaging over bi-weekly timescales. This suggests that WRF-Chem may be better able to capture the bi-weekly NH_3 averages than the short-term variability. Simulations consistently overestimated NH_3 mixing ratios at WI07. They were 59%, 40%, and 48% higher than observations for 2017, 2018, and 2019 respectively, but displayed no consistent systematic bias for the other sites. As discussed earlier, WI07 is classified as a remote site, but in fact is subject to significant agricultural influence with much higher NH_3 than the remote site MN18 (Figures S1 and S7). It is also located at the east boundary of the agricultural domain (Figure 1a). The persistent model bias at this site suggests an *a priori* NH_3 emission overestimate or deposition underestimate for this locale. Averaging over all AMoN sites, the simulations were biased low on average during May (48% lower than the observations for the 3 years) and June (13% lower), very similar to the tall tower results (Figures 1c–1e). Conversely, the simulations exhibited a high bias in August (44% higher) and September (23% higher).

The WRF-Chem low NH_3 bias during May and June could be driven by one or more of the following errors: (1) overly strong simulated vertical mixing (or higher PBL overestimate); (2) overestimated NH_3 loss to dry deposition; (3) overestimated NH_3 loss to aerosol uptake; and/or (4) underestimated NH_3 emissions. Further, the model overestimate during August and September could similarly be explained by the converse of any of these. Our first hypothesis is that the EDGAR seasonality scaling is incorrect.

As shown in Figure S3, the modeled PBL variations are generally consistent with observed hourly, diurnal, and daily averages, with $R^2 = 0.64$ ($P < 0.001$), and relative bias around 10% for both periods for hourly comparisons. Additionally, the relative accuracy of $PM_{2.5}$ simulations also imply accurate PBL simulations because $PM_{2.5}$ concentrations are strongly affected by boundary layer height (Figure S4) (Liu et al., 2020). This suggests that PBL errors are not driving the WRF-Chem NH_3 underestimates during May to June and August to September. Although seasonal changes in canopy characteristics can influence deposition velocity, the simulated agricultural land NH_3 dry deposition velocities (hereafter V_d) in May to June were only slightly higher (12%, 6%, 7% in 2017, 2018, and 2019) than in August to September (Table S4), suggesting that deposition is not likely driving the May to June model underestimates and August to September overestimates. Lastly, the simulated and observed NH_4NO_3 for the three EPA operated sites (https://aqs.epa.gov/api) (Figure S8), were similar and relatively low (generally less than 0.5 $\mu g/m^3$, equal to 0.14 ppb NH_3 and relatively small compared with atmospheric NH_3) when compared with observed and simulated gaseous NH_3 (Figure S5). We conclude, therefore, that the seasonal model bias in NH_3 is driven by errors in the *a priori* emissions. This likely reflects an underrepresentation of the agriculture/fertilizer NH_3 source, since

synthetic fertilizer is applied regionally during May and June with dynamic environmental factors, including air temperature, driving volatilization rates. These findings align with that of Paulot et al. (2014) who attributed a spring emission peak to corn fertilization; those of Zhang et al. (2012) who concluded that NH_3 emissions were highest from May to July based on multiple observational constraints; and Zhu et al. (2013) who concluded that US NH_3 emissions in spring were systematically underestimated when EDGAR seasonality was applied to the NEI inventory.

3.3. Constraining Monthly NH_3 Emissions

We next apply the model-measurement comparisons to develop an observation-informed estimate of regional NH_3 emissions. We adjusted the NH_3 emissions and investigated the relationship between NH_3 emissions and ground-level NH_3 mixing ratios. An additional modeling case was conducted for June to August and is defined as the "base case." Here, we used the annual averaged emission from NEI (adjusted for the year using the EPA emission trends), but did not use the EDGAR monthly trends as in the previous case. The simulations from the base case are compared with the original simulated case, hereafter defined as the seasonal case, which used scaled monthly emission factors (Tables S1 and S5). While the NH_3 mixing ratio changes between these simulations exhibit some spatial heterogeneity (Figures S9–S11), when averaged over the two main land use categories in the region (forests and agriculture), the fractional mixing ratio changes were highly similar to the corresponding emission changes. Specifically, in the seasonal case, averaged NH_3 mixing ratios increased over the base case by factors of 1.44 (June), 1.55 (July), and 1.32 (August) over agricultural regions and by factors of 1.39 (June), 1.54 (July), and 1.47 (August) over forested regions. These values are all within 10% of the corresponding monthly emission scale factors of 1.47, 1.64, and 1.35 (Table S1). As discussed below, the majority of NH_x is in the gas phase during spring to fall period in the Upper Midwest and deposition rates do not vary much temporally. This near-linear dependence of ground-level NH_3 mixing ratios on emissions indicates that the model-measurement concentration ratios at the AMoN sites can be used to estimate a *posteriori* NH_3 emissions at the landscape scale, and the value of 10% indicates potential uncertainty for derived NH_3 emissions.

To give more reliable uncertainty of derived NH_3 emissions, we need to consider other factors especially for simulated NH_3 dry deposition or ammonium particles. Previous work by Li et al. (2016) compared simulated V_d by two different methods across the US and found a 1.9-folder difference. However, our previous flux-gradient based observations indicated that the dry deposition is 30%–40% of gross NH_3 emissions (Griffis et al., 2019), and is consistent with simulated values of 41% for agricultural areas in this study. Further, as discussed later in Section 3.4, our simulated dry deposition in the Upper Midwest also showed high consistency with the independent results from Li et al. (2016). As shown in Figure S8, the mass density of both observed and simulated particles were $< 0.5\ \mu g/m^3$ for NH_4NO_3 particles and $<1\ \mu g/m^3$ for $(NH_4)_2SO_4$, which is equivalent to 0.1 and 0.3 ppb of gaseous NH_3, respectively. If we assume the relative uncertainty in NH_4NO_3 and $(NH_4)_2SO_4$ particles is as large as 50%, the resulting gaseous NH_3 biases are <1% and <3% and relatively small compared to the observed NH_3 mixing ratios (>6 ppb as shown in Figures S5 and S6). The potential uncertainties caused by NH_4^+ particles within the agricultural NH_3 dominated region are within the uncertainty (20%) for the retrieved NH_3 emissions. Further, Li et al. (2016) reported that the dry deposition of NH_4^+ was <5% of dry deposition for gaseous NH_3. Their observations further support our conclusions that the simulation of NH_4^+ particles has a very small influence on the constraint of NH_3 emissions. Even with the good performance of the above mentioned NH_3 dry deposition and relatively low NH_4^+ particle mass concentration for the study period, we attributed a value of 20% as the uncertainty of the derived NH_3 emissions.

We derive the *a posteriori* emission scaling factors by regressing the model output against the AMoN ground-level NH_3 observations. Least squares based regression slopes were calculated using 3 years of growing season AMoN data, with the corresponding scaling factors derived as the inverse of the slope (Figure S12, Table S6) (Bie et al., 2018; Fu et al., 2017). The mean scaling factors were 1.05 ± 0.21, 1.80 ± 0.38, 1.21 ± 0.05, 0.97 ± 0.08, 0.70 ± 0.01, 0.85 ± 0.03 for April, May, June, July, August, and September, respectively. Note that the standard deviation among the averaged three years represents an uncertainty of about 20%, which reflects the influence of interannual variations in emissions. For April and July, the mean

Table 1
Scaling Factors for the a Priori and Posteriori Monthly Scaling Factors From April to September for 3 Years

		April	May	June	July	August	September
Regression slopes	2017	0.76	0.56	0.84	0.94	1.41	1.16
	2018	1.24	0.44	0.86	1.15	1.44	1.13
	2019	0.99	0.74	0.78	1.03	1.45	1.23
Inverse of slopes		1.05 (±0.21)	1.80 (±0.38)	1.21 (±0.05)	0.97 (±0.08)	0.70 (±0.01)	0.85 (±0.03)
Priori scaling factors		1.09	1.02	1.47	1.64	1.35	1.03
Posteriori scaling factors		1.14 (±0.2)	1.75 (±0.4)	1.76 (±0.3)	1.64 (±0.3)	0.95 (±0.2)	0.88 (±0.2)
Posteriori NH_3 emission	Agricultural	2.91 (±0.6)	4.45 (±0.9)	4.47 (±0.9)	4.17 (±0.8)	2.41 (±0.5)	2.23 (±0.4)
	Forested	0.07 (±0.02)	0.11 (±0.03)	0.11 (±0.03)	0.10 (±0.03)	0.06 (±0.02)	0.05 (±0.02)

Note. The unit for emissions is nmol m^{-2} s^{-1}. A 20% uncertainty should be considered for the derived scaling factors, *Posteriori* scaling factors and *Posteriori* NH3 emissions.

scaling factors were close to 1, suggesting almost unbiased model simulations. While for May and June, the results suggested a large model underestimate of both NH_3 emissions and mixing ratios, and a model overestimate for August and September. The resulting *a posteriori* emission scaling factors with respect to the base case simulation indicates an emission peak between May and June, with scaling factors reaching 1.76 (Table 1). By applying the monthly *a posteriori* emission scaling factors to the *a priori* NEI NH_3 emissions, we derived the *posteriori* NH_3 emissions. These results indicate that growing season averaged NH_3 emissions for agricultural regions were 3.64 ± 0.7, 3.46 ± 0.7, and 3.27 ± 0.7 nmol m^{-2} s^{-1} for 2017, 2018, and 2019, respectively, and also suggest significant monthly variations in NH_3 emissions-especially for the agricultural areas. The *posteriori* emission rates for agricultural lands were low in April (2.91 ± 0.6 nmol m^{-2} s^{-1}), much higher from May to July (4.17 ± 0.8–4.47 ± 0.9 nmol m^{-2} s^{-1}), and then lower for August (2.41 ± 0.5 nmol m^{-2} s^{-1}) and September (2.23 ± 0.4 nmol m^{-2} s^{-1}). The *posteriori* emission peaks in May to June and the *a priori* emissions peak in July. A recent inversion study in China also found that the agricultural NH_3 emissions peak in May to June for Northeast and Northwest China, which has a similar climate as our study area (Kong et al., 2019).

3.4. Interannual Variability of NH_3 Dry Deposition

The majority of the US Corn Belt is contained within model Domain 2 and is dominated by agricultural lands (63%), which are concentrated in the southwest. Natural forests and grasslands occupy 21% of the remaining area within Domain 2. Since the study domain contains agricultural and natural land types, it can be used to investigate the influence of agricultural NH_3 emissions on NH_3 deposition to natural vegetation. Here, we investigate deposition using the *posteriori* case described above and applied the *posteriori* scaling factors to calibrate simulated NH_3 mixing ratio and dry deposition from the *a priori* cases (Figure 2). Overall, the relative standard deviation of NH_3 dry deposition is relatively low in the US Corn Belt, with the largest values near emission sources, indicating small interannual variations of NH_3 dry deposition (Figures 2a and S13). These values are generally smaller than 10% for agricultural lands, slightly smaller than forests/grasslands (i.e., 10%–30%) especially near the Great Lakes.

Land use partitioned spatial distributions of the net NH_3 flux were also determined for 2017–2019 for the *posteriori* case (Figure 2b). Here, net NH_3 sink and NH_3 source regions are clearly established. These regions are closely associated with land use. We attributed >97% of these differences to NH_3 emissions, rather than differences in V_d between agricultural and forest lands. Interestingly, sink regions near transition zones, like that observed in north-central Minnesota, experience larger depositional fluxes than sink regions further from sources. To further examine the differences between these land uses, NH_3 mixing ratios, V_d, dry deposition, and NH_4^+ mixing ratios were averaged by land use, month, and year (Figures 2c–2f).

Because the dry deposition simulation is the product of NH_3 mixing ratio and deposition velocity, we first examine the averaged *posteriori* NH_3 mixing ratios from the growing season for agricultural lands, which

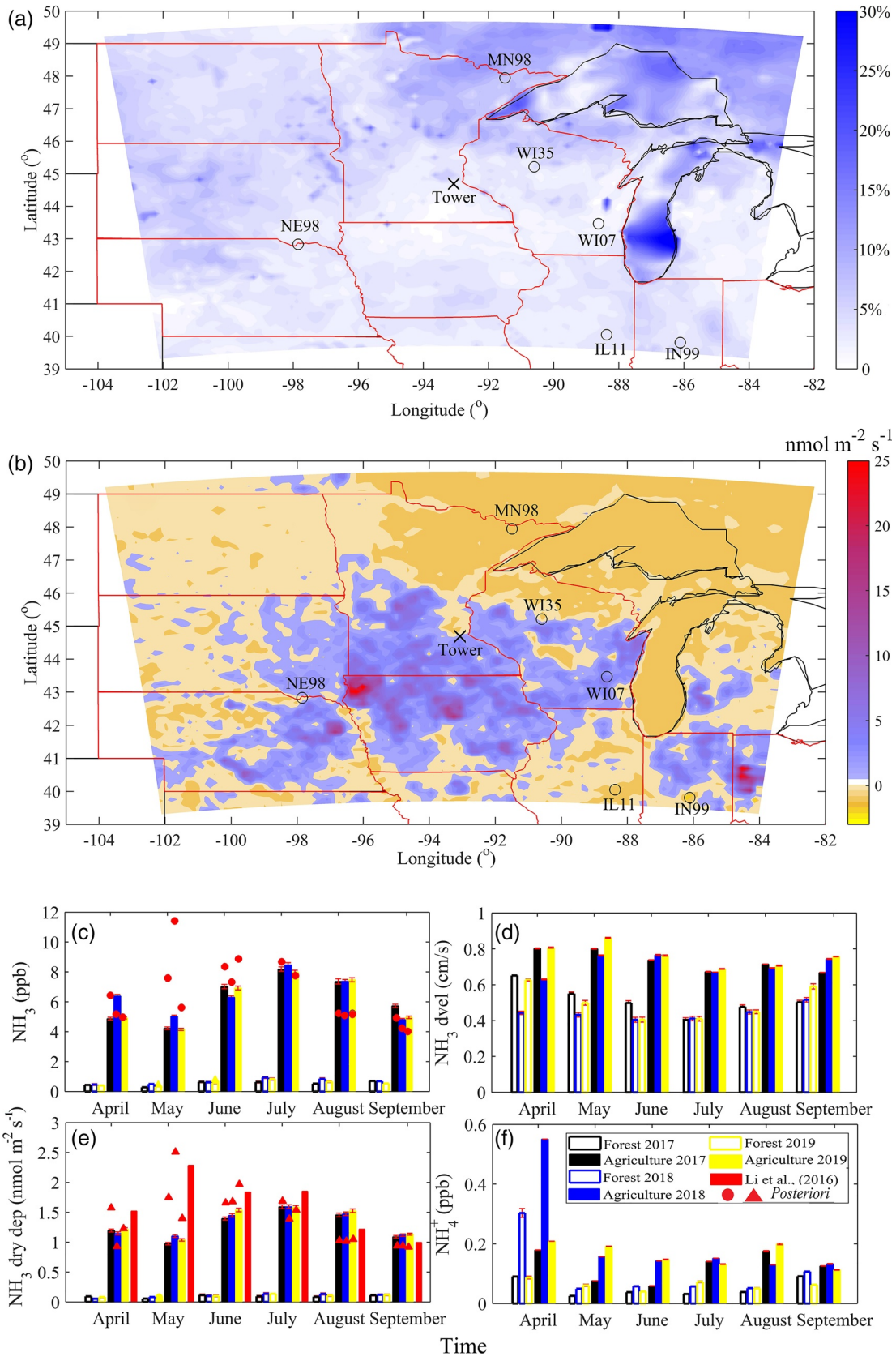
(a)
MN98
WI35
Tower
NE98
WI07
IL11
IN99
Latitude (°)
Longitude (°)
30%
25%
20%
15%
10%
5%
0
(b)
nmol m-2 s-1
MN98
WI35
Tower
NE98
WI07
IL11
IN99
Latitude (°)
Longitude (°)
(c)
NH3 (ppb)
(d)
NH3 dvel (cm/s)
(e)
NH3 dry dep (nmol m-2 s-1)
(f)
NH4+ (ppb)
April May June July August September
Time
Forest 2017
Agriculture 2017
Forest 2018
Agriculture 2018
Forest 2019
Agriculture 2019
Li et al., (2016)
Posteriori

were 6.87 ± 1.4, 6.76 ± 1.4, and 6.48 ± 1.3 ppb for 2017, 2018, and 2019, and were 0.58 ± 0.12, 0.71 ± 0.14, and 0.60 ± 0.12 ppb for forested lands. These results indicate small interannual variations between these 3 years, while there is remarkable monthly variations observed in May with the highest NH_3 mixing ratios in 2018 for agricultural lands. This was also evident in both the tall tower and ground-level NH_3 observations (Figures 1b and 1d). Domain averaged surface temperature in May was 12.7°C for 2017, 15.2°C for 2018 and 11.6°C for 2019. These higher temperatures would cause higher NH_3 emissions through increases in surface volatilization and lower deposition velocities (Sutton et al., 2013; Zhang et al., 2018), which likely contributed to the higher ambient NH_3 mixing ratios in 2018. Larger NH_3 emissions and NH_3 mixing ratios are projected with future air temperature increasing by > 1°C in 2050 for this region (Griffis et al., 2017, 2019). The relatively lower NH_3 emissions in May 2019 compared to the other 2 years can be attributed to the delayed crop planting caused by wetter and cooler conditions (Yin et al., 2020). Further, the higher NH_3 emissions in June 2019 compared to the previous 2 years suggests a shift of fertilizer application to a later date.

In the *posteriori* results, NH_3 mixing ratios were the highest in May and June, when fertilizer application and higher surface temperatures induced increases in NH_3 volatilization. The largest relative standard deviations in the mixing ratios occurred in May (Figure 2c). Simulated NH_3 mixing ratios for agricultural regions decreased in August and September. These decreases can be partially attributed to time elapsed since fertilizer application. As observed in Griffis et al. (2019), tall tower flux-gradients revealed a first peak in spring (most pronounced in May) and a second peak during fall (pronounced in November). This is consistent with the model analyses found here, with spring NH_3 emission increasing in May and lasting for three months, while the *a priori* NH_3 emissions began to peak in June. This 1-month time-shift helps to explain the overestimation of NH_3 emissions in August and September.

The simulated results for NH_3 mixing ratio, dry deposition velocity and flux in Figures 2c–2e indicate that NH_3 dry deposition flux was primarily controlled by NH_3 mixing ratio variations, rather than V_d, at both monthly and annual scales. To evaluate the NH_3 dry deposition flux for forested and agricultural lands, monthly fluxes were calculated for the *posteriori* case (displayed in red triangles and dots) and also for the *a priori* (Figures 2c–2f displayed in bars). For the *posteriori* case, the results were 1.44 ± 0.3 nmol m^{-2} s^{-1} in 2017, 1.42 ± 0.3 nmol m^{-2} s^{-1} in 2018, and 1.43 ± 0.3 nmol m^{-2} s^{-1} in 2019 for agricultural lands. Significant differences were evident between the *posteriori* and *a priori* cases. Our results are consistent with previous studies during the growing season in the Upper Midwest (Figure 2e, in red bars). Li et al. (2016) combined multiple observations with a land surface model and reported a growing season averaged dry deposition flux of 1.62 nmol m^{-2} s^{-1}. This favorable comparison further supports the use of the monthly *posteriori* NH_3 emissions for these agricultural lands. For forested lands, the dry deposition was 0.10 ± 0.01 nmol m^{-2} s^{-1} in 2017, 0.11 ± 0.02 nmol m^{-2} s^{-1} in 2018, and 0.11 ± 0.02 nmol m^{-2} s^{-1} in 2019. This deposition was slightly (~10%) higher than its emissions with relatively small annual variations. Interestingly, the relative variation in the spatial distribution of deposition for forested regions is larger than for agricultural regions, as illustrated in Figure 2a. This further supports that deposition in this region is more sensitive to atmospheric transport processes, because agricultural NH_3 sources can be transported to forested lands though long-distance transport.

4. Conclusions

Three years of tall tower hourly NH_3 mixing ratios and AMoN ground-level bi-weekly observations were used in combination with WRF-Chem to constrain NH_3 fluxes in the US Corn Belt. We evaluated the monthly and annual variations of NH_3 mixing ratios, emissions and dry deposition, and investigated the transport of NH_3 from agricultural lands to natural vegetation. The comparison between tall tower observations and model results indicate that *a priori* emissions were biased low for the months of May and June and biased high in August and September. *Posteriori* scaling factors of 1.6–1.7 should be applied for May and June to more accurately account for NH_3 emissions when using NEI 2011. During these months, synthet-

Figure 2. (a) Spatial distribution of the relative standard deviation of the NH_3 dry deposition flux for 2017 to 2019, (b) Spatial distribution of net NH_3 flux (i.e., emission minus dry deposition) for growing season averaged over 3 years, (c) NH_3 mixing ratios, (d) deposition velocity, V_d, (e) NH_3 dry deposition, and (f) NH_4^+ corresponding to agricultural and natural forest areas for the years 2017–2019. Note that the *posteriori* results are displayed in red triangles and dots.

ic fertilizer is widely applied to agricultural lands, suggesting this remains a significantly underestimated source in existing inventories. High NH_3 mixing ratios observed in May 2018 compared to other months was attributed to abnormal higher NH_3 emissions that were induced by a 2.5°C–3.6°C higher air temperature. This agricultural region acts as a net NH_3 source, with adjacent forested lands acting as a substantial net NH_3 sink. Forested lands received more NH_3 (~10%) from deposition compared to its emissions. This was caused by transportation from upwind agricultural sources. We estimate that the averaged agricultural NH_3 emissions and dry deposition were 3.45 ± 0.7 and 1.43 ± 0.3 nmol m^{-2} s^{-1}, respectively for the 2017–2019 growing seasons.

Data Availability Statement

The data presented in this manuscript is available at www.biometeorology.umn.edu/research/data-archives and ESS-DIVE (Deep Insights for Earth Science Data, https://data.ess-dive.lbl.gov/view/doi:10.15485/1550921).

Acknowledgments
This research was partially supported by the National Science Foundation (grant number 1640337), the United States Department of Agriculture National Institute of Food and Agriculture (USDA NIFA grant number 2018-67019-27808), USDA Agricultural Research Service, and the Minnesota Supercomputing Institute for Advanced Computational Research. Jeffrey D. Wood acknowledges support from the US Department of Energy, Office of Science, Office of Biological and Environmental Research Program, through Oak Ridge National Laboratory's Terrestrial Ecosystem Science Scientific Focus Area; ORNL is managed by UT-Battelle, LLC, for the US DOE under contract DE-AC05-00OR22725. Finally, we acknowledge use of the National Atmospheric Deposition Program databases.

References

Ackerman, D., Millet, D. B., & Chen, X. (2019). Global Estimates of Inorganic Nitrogen Deposition Across Four Decades. *Global Biogeochemical Cycles*, *33*(1), 100–107. https://doi.org/10.1029/2018GB005990

Balasubramanian, S., Koloutsou-Vakakis, S., McFarland, D. M., & Rood, M. J. (2015). Reconsidering emissions of ammonia from chemical fertilizer usage in Midwest USA. *Journal of Geophysical Research: Atmospheres*, *120*(12), 6232–6246. https://doi.org/10.1002/2015JD023219

Balasubramanian, S., Nelson, A., Koloutsou-Vakakis, S., Lin, J., Rood, M. J., Myles, L., & Bernacchi, C. (2017). Evaluation of DeNitrification DeComposition model for estimating ammonia fluxes from chemical fertilizer application. *Agricultural & Forest Meteorology*, *237–238*, 123–134. https://doi.org/10.1016/j.agrformet.2017.02.006

Bash, J. O., Cooter, E. J., Dennis, R. L., Walker, J. T., & Pleim, J. E. (2013). Evaluation of a regional airquality model with bidirectional NH_3 exchange coupled to an agroecosystem model. *Biogeosciences*, *10*(3), 1635–1645. https://doi.org/10.5194/bg-10-1635-2013

Bie, N., Lei, L., Zeng, Z., Cai, B., Yang, S., He, Z., et al. (2018). Regional uncertainty of GOSAT XCO_2 retrievals in China: Quantification and attribution. *Atmospheric Measurement Techniques*, *11*(3), 1251–1272. https://doi.org/10.5194/amt-11-1251-2018

Bouwman, L., Goldewijk, K. K., Van Der Hoek, K. W., Beusen, A. H. W., Van Vuuren, D. P., Willems, J., et al. (2013). Exploring global changes in nitrogen and phosphorus cycles in agriculture induced by livestock production over the 1900–2050 period. *Proceedings of the National Academy of Sciences*, *110*(52), 20882–20887. https://doi.org/10.1073/pnas.1012878108

Dammers, E., Mclinden, C. A., Griffin, D., Shephard, M. W., Graaf, S. V. D., Lutsch, E., et al. (2019). NH_3 emissions from large point sources derived from CrIS and IASI satellite observations. *Atmospheric Chemistry and Physics*, *19*(19), 12261–12293.

Dammers, E., Schaap, M., Haaima, M., Palm, M., Wichink Kruit, R. J., Volten, H., et al. (2017). Measuring atmospheric ammonia with remote sensing campaign: Part 1 – Characterisation of vertical ammonia concentration profile in the centre of The Netherlands. *Atmospheric Environment*, *169*, 97–112. https://doi.org/10.1016/j.atmosenv.2017.08.067

EPA (2014). https://edap.epa.gov/public/extensions/nei_report_2014/

Fu, C., Lee, X., Gri, T. J., Dlugokencky, E. J., & Andrews, A. E. (2017). Investigation of the N_2O emission strength in the U. S. Corn Belt. *Atmospheric Research*, *194*, 66–77. https://doi.org/10.1016/j.atmosres.2017.04.027

Galloway, J. N., Townsend, A. R., Erisman, J. W., Bekunda, M., Cai, Z., Freney, J. R., et al. (2008). Transformation of the nitrogen cycle: Recent trends, questions, and potential solutions. *Science*, *320*(5878), 889–892. https://doi.org/10.1126/science.1136674

Gilliland, A. B., Dennis, R. L., Roselle, S. J., & T. E. P. (2003). Seasonal NH_3 emission estimates for the eastern United States based on ammonium wet concentrations and an inverse modeling method. *Journal of Geophysical Research*, *108*(D15), 4477. https://doi.org/10.1029/2002JD003063

Goebes, M. D., Strader, R., & Davidson, C. (2003). An ammonia emission inventory for fertilizer application in the United States. *Atmospheric Environment*, *37*(18), 2539–2550. https://doi.org/10.1016/S1352-2310(03)00129-8

Green, T. R., Kipka, H., David, O., & Mcmaster, G. S. (2017). Where is the USA Corn Belt, and how is it changing ? *Science of the Total Environment*, *618*, 1613–1618. https://doi.org/10.1016/j.scitotenv.2017.09.325

Griffis, T. J., Chen, Z., Baker, J. M., Wood, J. D., Millet, D. B., & Lee, X. (2017). Nitrous oxide emissions are enhanced in a warmer and wetter world. *Proceedings of the National Academy of Sciences*, *114*(45), 12081–12085. https://doi.org/10.1073/pnas.1704552114

Griffis, T. J., Hu, C., Deventer, M. J., & Winker, C. (2019). Tall Tower Ammonia Observations and Emission Estimates in the U.S. Midwest. *Journal of Geophysical Research: Biogeosciences*, *124*(11), 3432–3447. https://doi.org/10.1029/2019JG005172

Heald, C. L., Collett, J. L., Lee, T., Benedict, K. B., Schwandner, F. M., Li, Y., et al. (2012). Atmospheric ammonia and particulate inorganic nitrogen over the United States. *Atmospheric Chemistry and Physics*, *12*(21), 10295–10312. https://doi.org/10.5194/acp-12-10295-2012

Hu, C., Griffis, T. J., Baker, J. M., Wood, J. D., Millet, D. B., Yu, Z., & Lee, X. (2019). Modeling the Sources and Transport Processes During Extreme Ammonia Episodes in the U.S. Corn Belt. *Journal of Geophysical Research: Atmospheres*, *125*(2), e2019JD031207. https://doi.org/10.1029/2019JD031207

Kong, L., Tang, X., Zhu, J., Wang, Z., Xie, Y., Liu, Z., & Sui, W. (2019). Improved Inversion of Monthly Ammonia Emissions in China Based on the Chinese Ammonia Monitoring Network and Ensemble Kalman Filter. *Environmental Science & Technology*, *53*(21), 12529–12538. https://doi.org/10.1021/acs.est.9b02701

Li, Y., Schichtel, B. A., Walker, J. T., Schwede, D. B., Chen, X., Lehmann, C. M. B., et al. (2016). Increasing importance of deposition of reduced nitrogen in the United States. *Proceedings of the National Academy of Sciences*, *113*(21), 5874–5879. https://doi.org/10.1073/pnas.1525736113

Liu, C., Huang, J., Wang, Y., Tao, X., Hu, C., Deng, L., et al. (2020). Vertical distribution of $PM_{2.5}$ and interactions with the atmospheric boundary layer during the development stage of a heavy haze pollution event. *Science of The Total Environment*, *704*, 135329. https://doi.org/10.1016/j.scitotenv.2019.135329

Moravek, A., Murphy, J. G., Hrdina, A., Lin, J. C., Pennell, C., Franchin, A., et al. (2019). Wintertime spatial distribution of ammonia and its emission sources in the Great Salt Lake region. *Atmospheric Chemistry and Physics*, *19*(24), 15691–15709. https://doi.org/10.5194/acp-19-15691-2019

Olivier, J. G. J., Bouwman, A. F., Van der Maas, C. W. M., & Berdowski, J. J. M. (1994). Emission Database for Global Atmospheric Research (EDGAR). *Environmental Monitoring and Assessment*, *31*(1–2), 93–106.

Paulot, F., Jacob, D. J., Pinder, R. W., Bash, J. O., Travis, K., & Henze, D. K. (2014). Ammonia emissions in the United States, European Union, and China derived by high-resolution inversion of ammonium wet deposition data: Interpretation with a new agricultural emissions inventory (MASAGE_NH3). *Journal of Geophysical Research: Atmospheres*, *119*(7), 4343–4364. https://doi.org/10.1002/2013JD021130

Schiferl, L. D., Heald, C. L., Damme, M. V., Clarisse, L., Clerbaux, C., Coheur, P., et al. (2016). Interannual variability of ammonia concentrations over the United States: Sources and implications. *Atmospheric Chemistry and Physics*, *16*(18), 12305–12328. https://doi.org/10.5194/acp-16-285

Sebestyen, S. D., Ross, D. S., Shanley, J. B., Elliott, E. M., Kendall, C., Campbell, J. L., et al. (2019). Unprocessed Atmospheric Nitrate in Waters of the Northern Forest Region in the U.S. and Canada. *Environmental Science & Technology*, *53*(7), 3620–3633. https://doi.org/10.1021/acs.est.9b01276

Sheppard, L. J., Leith, I. A. N. D., Mizunuma, T., & Cape, J. N. (2011). Dry deposition of ammonia gas drives species change faster than wet deposition of ammonium ions: Evidence from a long-term field manipulation. *Global Change Biology*, *17*(12), 3589–3607. https://doi.org/10.1111/j.1365-2486.2011.02478.x

Shonkwiler, K. B., & Ham, J. M. (2018). Ammonia emissions from a beef feedlot: Comparison of inverse modeling techniques using long-path and point measurements of fenceline NH_3. *Agricultural and Forest Meteorology*, *258*, 29–42. https://doi.org/10.1016/j.agrformet.2017.10.031

Sutton, M. A., Reis, S., Riddick, S. N., Dragosits, U., Nemitz, E., Theobald, M. R., et al. (2013). Towards a climate-dependent paradigm of ammonia emission and deposition. *Philosophical Transactions of the Royal Society B: Biological Sciences*, *368*(1621), 20130166–20130166. https://doi.org/10.1098/rstb.2013.0166

Tevlin, A. G., Li, Y., Collett, J. L., McDuffie, E. E., Fischer, E. V., & Murphy, J. G. (2017). Tall Tower Vertical Profiles and Diurnal Trends of Ammonia in the Colorado Front Range. *Journal of Geophysical Research: Atmospheres*, *122*(22), 12468–12487. https://doi.org/10.1002/2017JD026534

Walker, J. M., Philip, S., Martin, R. V., & Seinfeld, J. H. (2012). Simulation of nitrate, sulfate, and ammonium aerosols over the United States. *Atmospheric Chemistry and Physics*, *12*(22), 11213–11227. https://doi.org/10.5194/acp-12-11213-2012

Warner, J. X., Dickerson, R. R., Wei, Z., Strow, L. L., Wang, Y., & Liang, Q. (2017). Increased atmospheric ammonia over the world's major agricultural areas detected from space. *Geophysical Research Letters*, *44*(6), 2875–2884. https://doi.org/10.1002/2016GL072305

Yin, Y., Byrne, B., Liu, J., Wennberg, P. O., Davis, K. J., Magney, T., et al. (2020). Cropland Carbon Uptake Delayed and Reduced by 2019 Midwest Floods. *AGU Advances*, *1*(1), e2019AV000140. https://doi.org/10.1029/2019AV000140

Yu, F., Nair, A. A., & Luo, G. (2018). Long-Term Trend of Gaseous Ammonia Over the United States: Modeling and Comparison With Observations. *Journal of Geophysical Research: Atmospheres*, *123*(15), 8315–8325. https://doi.org/10.1029/2018JD028412

Zaveri, R. A., Easter, R. C., Fast, J. D., & Peters, L. K. (2008). Model for Simulating Aerosol Interactions and Chemistry (MOSAIC). *Journal of Geophysical Research*, *113*(D13). https://doi.org/10.1029/2007JD008782

Zhang, L., Chen, Y., Zhao, Y., Henze, D. K., Zhu, L., Song, Y., et al. (2018). Agricultural ammonia emissions in China: reconciling bottom-up and top-down estimates. *Atmospheric Chemistry and Physics*, *18*, 339–355. https://doi.org/10.5194/acp-18-339-2018

Zhang, L., Jacob, D. J., Knipping, E. M., Kumar, N., Munger, J. W., Carouge, C. C., et al. (2012). Nitrogen deposition to the United States: Distribution, sources, and processes. *Atmospheric Chemistry and Physics*, *12*(10), 4539–4554. https://doi.org/10.5194/acp-12-4539-2012

Zhu, L., Henze, D. K., Cady-Pereira, K. E., Shephard, M. W., Luo, M., Pinder, R. W., et al. (2013). Constraining U.S. ammonia emissions using TES remote sensing observations and the GEOS-Chem adjoint model. *Journal of Geophysical Research: Atmospheres*, *118*(8), 3355–3368. https://doi.org/10.1002/jgrd.50166

References from the Supporting Information

Cooter, E. J., Bash, J. O., Benson, V., & Ran, L. (2012). Linking agricultural crop management and air quality models for regional to national-scale nitrogen assessments. *Biogeosciences*, *9*(10), 4023–4035. https://doi.org/10.5194/bg-9-4023-2012

Lonsdale, C. R., Hegarty, J. D., Cady-Pereira, K. E., Alvarado, M. J., Henze, D. K., Turner, M. D., et al. (2017). Modeling the diurnal variability of agricultural ammonia in Bakersfield, California, during the CalNex campaign. *Atmospheric Chemistry and Physics*, *17*(4), 2721–2739. https://doi.org/10.5194/acp-17-2721-2017

Pleim, J. E., Bash, J. O., Walker, J. T., & Cooter, E. J. (2013). Development and evaluation of an ammonia bidirectional flux parameterization for air quality models. *Journal of Geophysical Research: Atmospheres*, *118*(9), 3794–3806. https://doi.org/10.1002/jgrd.50262